Chemically grafted fibronectin for use in QCM-D cell studies

Judith Kandel [a,1], Hyun-Su Lee [b,d,1], Peter Sobolewski [d,2], Nancy Tomczyk [d],
Russell J. Composto [b,c], David M. Eckmann [a,c,d,*]

[a] Department of Bioengineering, University of Pennsylvania, Philadelphia, PA 19104, USA
[b] Department of Materials Science and Engineering, University of Pennsylvania, Philadelphia, PA 19104, USA
[c] Institute for Medicine and Engineering, University of Pennsylvania, Philadelphia, PA 19104, USA
[d] Department of Anesthesiology and Critical Care, University of Pennsylvania, 331 John Morgan Building, 3620 Hamilton Walk, Philadelphia, PA 19104, USA

ARTICLE INFO

ABSTRACT

Traditionally, fibronectin has been used as a physisorbed surface coating (physFN) in cell culture experiments due to its critical role in cell adhesion. However, because the resulting layer is thick, unstable, and of unpredictable uniformity, this method of fibronectin deposition is unsuitable for some types of research, including quartz crystal microbalance (QCM) experiments involving cells. Here, we present a new method for chemical immobilization of fibronectin onto silicon oxide surfaces, including QCM crystals pre-coated with silicon oxide. We characterize these chemically coated fibronectin surfaces (chemFN) as well as physFN ones using spectroscopic ellipsometry (SE), Fourier transform infrared spectroscopy (FTIR), atomic force microscopy (AFM), and contact angle measurements. A cell culture model demonstrates that cells on chemFN and physFN surfaces exhibit similar viability, structure, adhesion and metabolism. Finally, we perform QCM experiments using cells on both surfaces which demonstrate the superior suitability of chemFN coatings for QCM research, and provide real-time QCM-D data from cells subjected to an actin depolymerizing agent. Overall, our method of chemical immobilization of fibronectin yields great potential for furthering cellular experiments in which thin, stable and uniform coatings are desirable. As QCM research with cells has been rather limited in success thus far, we anticipate that this new technique will particularly benefit this experimental system by availing it to the much broader field of cell mechanics.

© 2014 Elsevier B.V. All rights reserved.

1. Introduction

Biological surface coatings constitute a major area of research for the purposes of both medical device applications and improvements in biomedical research techniques. Advances in medical device surface modification include our group's recent work on the antibacterial properties and hemocompatibility of grafted surfaces (Coll Ferrer et al., 2013; Dastgheyb et al., 2013; Eckmann et al., 2013; Lee et al., 2013a, 2013b), with many other new developments reviewed by (Campoccia et al., 2013) and (Meyers and Grinstaff, 2012). Emerging technologies in biological research also often require the grafting of biomaterials, including various protein coatings to enable cell and biomolecule attachment in

microfluidic devices (Shirtcliffe et al., 2013) and even the immobilization of enzymes for biocatalysis performance (Jia et al., 2014).

One particular biomolecule often used to promote cell attachment is fibronectin, a critical component of the extracellular matrix (ECM) which has binding sites to cellular integrins, heparin, collagen and fibrin (Pankov and Yamada, 2002). It usually exists as a dimer of two monomers, each containing three types of repeating subunits. The third subunit contains the RGD peptide, a tripeptide arginine–glycine–aspartic acid sequence. This is the primary binding site for α5 integrins (Pierschbacher et al., 1984; Pytela et al., 1985; Takada et al., 1987), transmembrane receptors which mediate cell adhesion to substrates, such as neighboring cells and the ECM. In addition to preventing a particular type of apoptosis deemed anoikis (Frisch, 1996), integrins are heavily involved in various cell signaling mechanisms, such as enhancing cell proliferation, governing platelet activation, and directing cell migration (Miranti and Brugge, 2002).

Because of fibronectin's important role in cell adhesion, it has been used extensively as a thin surface coating in cell culture experiments by our laboratories and many others (Klinger et al., 2011; Toworfe et al. 2009; Ostuni et al., 2000; Ingber and Folkman, 1989; Uttayarat et al., 2010). These coatings are physically absorbed

* Corresponding author at: Department of Anesthesiology and Critical Care, 331 John Morgan Building, 3620 Hamilton Walk, Philadelphia, PA 19104, USA.
Tel.: +1 215 746 1482; fax: +1 215 349 5078.
E-mail address: David.Eckmann@uphs.upenn.edu (D.M. Eckmann).
[1] These authors contributed equally to this work.
[2] Present address: Department of Chemical Technology and Engineering, Division of Biomaterials and Microbiological Technologies, West Pomeranian University of Technology, Szczecin, 45 Piastów Avenue, Szczecin 70-311, Poland.

to existing surfaces (physFN), with excess solution aspirated before cells are plated. While suitable for most research, the physical method of fibronectin deposition results in coatings that are too thick, nonuniform, and unstable for studies where these qualities are important. Such research includes the use of certain microfluidic devices and flow chambers (Kent et al., 2010), as well as quartz crystal microbalance (QCM) studies where cellular properties are of interest. QCM detects changes in resonance frequencies and dissipation (for quartz crystal microbalance with dissipation, QCM-D) of a quartz crystal oscillated by a shear wave resonator in order to model changes in mass and viscoelastic properties of the surface. Since decay length of the shear wave can be less than 250 nm (Fredriksson et al., 1998), the surface layer deposited on the crystal must be as thin as possible to maximize detection of mass or mechanical changes of cells resting on the substrate. In addition, substrate uniformity helps ensure that an observed effect is occurring to a similar degree across the crystal's surface area, a common assumption in QCM modeling (Vig and Ballato, 1998). Covalent attachment, rather than physical adsorption, of fibronectin would be more appropriate for such studies because it can provide an exceptionally thin, uniform and stable surface.

Previous QCM research involving cells has been limited, probably due in part to the challenges presented by physically coating QCM crystals for biofunctionalization. Thus far, most QCM studies involving cells have used QCM in order to sense and characterize cell adhesion to the crystal surface, and some have correlated changes in frequency with the known value of cell density (Fredriksson et al., 1998; Zhou et al., 2000; Modin et al., 2006). A significant subset of this research investigates changes in cell adhesion in response to substrate modification (reviewed by Saitakis and Gizeli, 2011). Several studies have gone one step further by investigating real-time mechanical changes in cells on QCM crystals in response to cytoskeleton-disrupting drugs (Saitakis et al., 2010; Marx et al., 2007). Only a few QCM research studies have used QCM for sensing both short- and long-term changes in cellular viscoelastic properties in more biologically relevant situations, and they tend to be limited. Elsom et al. (Elsom et al., 2008) used QCM to examine epithelial cell uptake of microspheres, and Chen et al. (2012) employed QCM to study the effects of epidermal growth factor on cell mechanics. These are reviewed along with other studies by Saitakis and Gizeli (2011) and Xi et al. (2013). In none of these studies is the QCM crystal functionalized as is traditionally done in cell culture experiments.

Changes in cellular mechanical properties are a critical feature of many cellular processes, such as stem cell differentiation (Titushkin and Cho, 2007; Darling et al., 2008), apoptosis (Pelling et al., 2009), and cancer (Cross et al., 2007), and currently there is considerable biomedical and bioengineering research focused on methods of measuring such changes. As such, the adaptation of QCM for this purpose is paramount.

Perhaps because of the drawbacks of physically coating surfaces with fibronectin, Völcker et al. (2001) demonstrated a way to functionalize silicon rubber in order to covalently attach fibronectin. Their technique involves grafting acrylic acid (AAc), methacrylic acid (MAAc), or glycidyl methacrylate (GMA) onto silicon substrates. GMA, immobilized using radical polymerization, provides the substrate with epoxy groups which easily bind fibronectin by reacting with primary amine groups on fibronectin's lysine residues. The radical polymerization method presents a significant drawback, however, as it creates an epoxide-functionalized layer with an indeterminate number of monomers and therefore varying thickness, which is unsuitable for applications requiring thin, uniform surfaces.

Here, we report a new method of chemically grafting fibronectin (chemFN) to silicon oxide surfaces. We improve upon Völcker et al.'s method by using 3-glycidoxypropyltrimethoxysilane (GPTMS) instead of GMA for epoxy functionalization, closely following our recently published work on grafting chitosan to silicon oxide surfaces (Lee et al., 2012b). This allows for the epoxide-containing molecules to covalently attach to glass, quartz or silicon surfaces in a characteristic single-molecule layer. Our laboratory has previously reported studies of physical adsorption of fibronectin onto various silane self-assembled monolayers (Toworfe et al., 2009), as well as the resulting effects on cell adhesion (Lee et al., 2006). This study is the first in which is described both the chemical grafting of fibronectin onto a GPTMS monolayer via a well-known epoxide–amine reaction (Hermanson, 1996) and the resultant grafted layer's particular suitability for cell-based research using QCM-D. We characterize the chemFN surface using surface ellipsometry (SE), atomic force microscopy (AFM) and QCM-D. In addition, we use human umbilical vein endothelial cells (HUVEC) to assess biocompatibility by measuring cell adhesion, viability, cytoskeletal structure and metabolic properties on both chemFN and physFN substrates. We then compare QCM-D sensitivity to the presence of cells on both surfaces, and study the effect of cell density on the average thickness, viscosity, and shear modulus of the adherent cell layer on the chemFN-coated crystal surface. Finally, we demonstrate that QCM-D can detect viscoelastic changes in fibroblasts subjected to cytochalasin D, an actin depolymerizing agent, when plated on chemFN coated crystals.

2. Materials and methods

2.1. Surface preparation and characterization

N-Type, (100) oriented silicon wafers (CZ silicon, dopant; Ph, 20–30 Ω resistivity) were purchased from Silicon Quest International. QCM sensor crystals, AT-cut piezoelectric quartz crystals (14 mm in diameter and 0.3 mm thickness) coated with a 50 nm thick layer of silicon dioxide, were purchased from Biolin Scientific, Inc. Microscope coverslips (24-40-1) were purchased from Fisher Scientific. Silicon wafers (20 mm $\times$ 20 mm for SE measurements), microscope coverslips (24 mm $\times$ 40 mm for cell culture), and SiO$_2$-coated QCM sensor crystals were cleaned by immersion in piranha solution (3:1 (v:v) H$_2$SO$_4$/30% H$_2$O$_2$ (Fisher Scientific)), rinsed with ultrapure water (Millipore Direct-Q, 18 MΩ cm resistivity), dried with N$_2$, and exposed to UV–ozone to produce a homogeneous hydroxylated surface and to remove impurities. GPTMS ($\geq$ 98%, Aldrich Chemical Co.) deposition on silicon oxide surfaces was performed by immersion of the wafers, coverslips, and crystals into 10% (v/v) GPTMS in anhydrous toluene (99.8%, Aldrich Chemical Co.) at 80 °C for 12 h under N$_2$. The deposited samples were sonicated in toluene to remove physically absorbed GPTMS and impurities on the surface. The GPTMS surface was then covered in a 10 μg/mL fibronectin (BD Biosciences) solution, water was evaporated slowly, and the fibronectin film was formed by direct contact with the GPTMS surface at 60 °C, overnight ($\sim$ 12 h). The surface was immersed in deionized (DI) water with shaking at 200 rpm for 1 day to remove physically adsorbed fibronectin and other surface impurities.

To prepare physFN layers, cleaned silicon oxide surfaces were immersed in a 50 μg/mL fibronectin solution for either 30 min or 12 h in a 37 °C incubator receiving 5% CO$_2$. The surfaces were gently rinsed (1 $\times$) with ultrapure water to remove loosely absorbed fibronectin and other surface impurities.

For surface characterization methods, including ellipsometry, Fourier transform infrared spectroscopy (FTIR), and atomic force microscopy, see Supplementary Material section.

2.2. Cell culture and viability assays

All cells and cell culture media for in vitro cell culture models were obtained from Lifeline Cell Technology (Walkersville, MD). HUVEC were cultured in VascuLife VEGF cell culture media as

previously described (Sobolewski et al., 2011). Cytochalasin D experiments used human dermal fibroblasts cultured in FibroLife cell culture media. Briefly, cells between passage 2 and 5 were plated onto sterilized chemFN and physFN surfaces approximately 48 h before planned experiments, or 3 h for adhesion experiments. Most cell experiments included control physFN surfaces which were coated at a fibronectin concentration of 50 μg/mL for 30–40 min before aspiration. All dye loading and incubation was performed in the dark.

We followed well-established procedures for cell metabolic activity assessment, actin staining, cell adhesion comparisons, measurement of cellular proliferative capacity, and assessment of intracellular calcium release following ATP stimulation. Explicit details concerning these methods as well as our fluorescence microscopy methods are provided in Supplementary Material section.

2.3. QCM-D experiments

The QCM-D measurement is based on the resonance frequency change of a vibrating quartz crystal, a piezoelectric material, in response to mass deposition. The deposited mass, Δm, is related to the frequency change, Δf_n, according to the Sauerbrey equation (Sauerbrey, 1959; Jhon et al., 2006):

$$\Delta m = -C(\Delta f_n/n) \tag{1}$$

where C is the mass sensitivity constant ($C = 17.7$ ng cm^{-2} Hz^{-1} for an AT-cut, 5 MHz crystal) and n is the vibrational mode number ($n = 1, 3, 5,…$). In addition, the dissipation change, ΔD_n, the loss of energy stored in a vibration cycle, indicates the mechanical characteristics of the deposited layer such as viscosity, elasticity, and so on. An elastic film has ΔD_n less than 2.0×10^{-6} and superimposable plots of $\Delta f_n/n$ under several modes; the Sauerbrey equation (Sauerbrey, 1959; Vogt et al., 2004) can be used to calculate the layer's mass and thickness. On the contrary, a viscoelastic layer has a ΔD_n of more than 2.0×10^{-6} and plots of $\Delta f_n/n$ which cannot be superimposed. The physical properties (thickness, shear modulus, and viscosity) of the layer can be estimated by fitting the QCM-D experimental data ($\Delta f_n/n$ and ΔD_n) to a Voigt-based viscoelastic model incorporated in Q-Sense software Q-Tools (Lee et al., 2011; Lee and Penn, 2008; Höök et al., 2001). An E4 QCM instrument (Q-Sense Inc., Gothenburg, Sweden) was used for all QCM-D experiments.

For stability assessments, chemFN and physFN coated sensors were monitored in the QCM-D instrument when subjected to DI water flowing at 40 μL/min for 24 h at 21 °C. For evaluation of the physFN and chemFN modified sensors containing cells, both sensors were first monitored for frequency and dissipation at 21 °C in PBS containing calcium and magnesium at a flow rate of 100 μL/min (stage I in Fig. 4 (a)). Data was collected when frequency and dissipation reached constant values. Then, crystals were removed from the QCM-D and sterilized with ethanol. Cells were plated on both crystals and placed in the incubator for approximately 48 h in cell culture media. Both QCM sensors were then reloaded into flow modules, and frequency and dissipation were measured in PBS using the same method as stage I (stage II in Fig. 4(a)). Cells were then stained with calcein-AM and imaged to demonstrate their viability and measure cell density on the crystal. Finally, a published oxygen plasma method (Lee et al., 2012a, 2012b) was used to remove the organic layer (in this case, the underlying fibronectin layer and the overlying adherent cell layer) of both sensors without damaging the underlying silicon oxide surface. The cleaned crystals were then reloaded (stage III in Fig. 4(a)) and frequency and dissipation data were collected using the same method as stage I. This allowed us to estimate the physical properties of the chemFN and physFN fibronectin layers (stage I).

Real-time cytochalasin D (cytD) experiments involved growing fibroblasts on chemFN coated crystals for 48 h and then placing single crystals into the QCM-D in PBS solution. When a baseline was obtained, the perfusate was switched to 0.1% DMSO and a new, stable baseline was obtained. Finally, a 1 μM solution of cytD (containing ~0.1% DMSO as a final concentration) in PBS was added. This stepwise progression in solutions enabled isolation of the cytD effects

2.4. Statistics

SigmaPlot (SysStat Inc., San Jose, CA) was used for data plotting and statistical analysis. Where appropriate, data are reported as mean ± standard deviation. A Student's t-test was used for comparing chemFN and physFN cells' calcium flashes in response to ATP stimulation. A paired Student's t-test was used for comparing adhesion and alamarBlue data from the two groups, since results varied across experiments. In all cases, $p < 0.05$ was considered significant.

3. Results and discussion

3.1. Immobilization of fibronectin on silicon oxide surfaces

The well-known epoxide–amine reaction was used to immobilize fibronectin onto silicon oxide surfaces, including microscope

Layer	Thickness (nm)	Contact angle (°)
GPTMS	0.9	41.1 ± 1.3
ChemFN	3.0 ± 0.5	53.3 ± 2.3
PhysFN[1]	3.5 ± 0.1	90.7 ± 1.6
PhysFN[2]	19.4 ± 2.0	104.7 ± 1.5
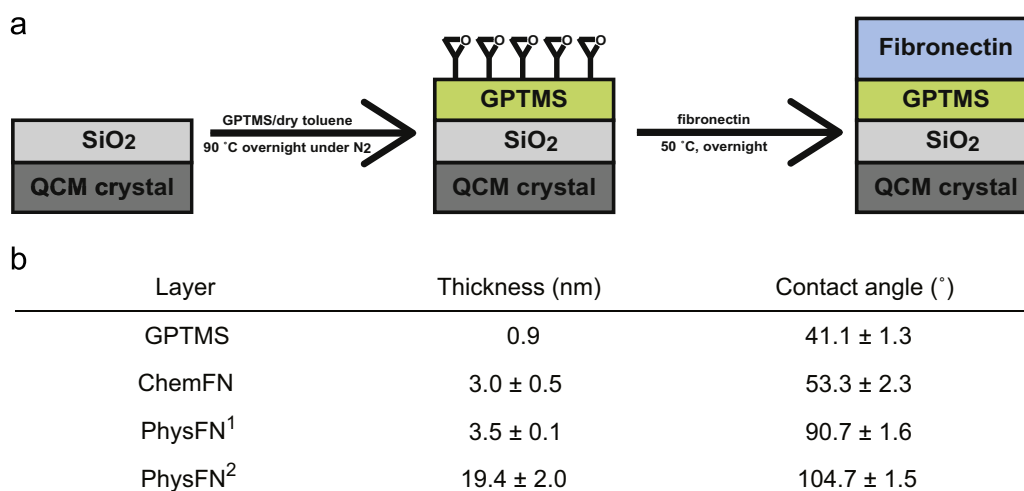
Fig. 1. (a) Experimental scheme of fibronectin immobilization onto silicon oxide surfaces, including glass microscope coverslips, hydroxylated silicon wafers, and silicon oxide coated QCM sensors, using the well-known epoxide–amine reaction. (b)Table displaying ellipsometric thickness and contact angle of dry layers. After [1]30 min and [2]12 h exposure of FN solution to SiO$_2$ surfaces, respectively, contact angle and thickness were measured between 3 and 5 times for each surface.

cover glasses, hydroxylated silicon wafers, and silicon oxide coated QCM sensors. Fig. 1(a) gives a graphic description of our method of chemical immobilization of fibronectin onto surfaces. First, silicon oxide surfaces were modified with epoxide functional groups by reacting trimethoxy silane groups of GPTMS and hydroxyl groups on silicon oxide surfaces. The thickness value measured by SE and the water contact angle of GPTMS derivatized layers (shown in the table in Fig. 1(b)) are in reasonable agreement with values obtained in the literature (Lee et al., 2012b, 2011). Upon fibronectin deposition, primary amine functional groups from lysines in fibronectin react with epoxide groups from GPTMS on the surface, resulting in stable covalent bonds.

Preliminary data showed that after the initial rinsing of the chemFN surfaces with DI water, further prolonged rinsing on a shaker had no effect on surface thickness as measured by ellipsometry (data not shown). PhysFN surfaces treated the same way became thinner by 16% in just 24 h (from 55.5 ± 1.6 nm to 46.6 ± 3.7 nm, $p = 0.012$), indicating that the fibronectin coating washed away over time. To more accurately capture the setting and chemistry involved in QCM experiments, we also performed rinsing in the QCM-D for 24 h. As Fig. S1 shows, the frequency and dissipation readings of the chemFN surface stabilize after several hours, while the physFN surface readings are still under flux after 24 h. The decreases in physFN frequencies, indicating mass adsorption, do not necessarily contradict the ellipsometry measurements showing thinning since the QCM-D experiments are done in solution while ellipsometry measures dry thickness. These data demonstrate the superior stability of chemFN surfaces to physFN ones, an imperative quality for QCM-D research, and propelled our further research involving chemFN surfaces in conjuction with QCM-D.

As shown in the table in Fig. 1(b), the chemFN grafted layer has a dry thickness of 3.0 nm and water contact angle of 53°. Fig. S2 shows contact angle measurements for chemFN and two different physFN surfaces. Since the contact angle value of chemFN is closer to that of GPTMS, and a reduced thickness is characteristic of a chemical rather than physical deposition, this data suggests that the fibronectin in chemFN is chemically grafted to the GPTMS derivatized surface. The chemFN layer is somewhat less hydrophilic than the GPTMS layer, which has a contact angle of 41°. The physFN[2] layer, which used a 12 h exposure of fibronectin solution to the SiO$_2$ surface, has a larger contact angle and dry thickness than the physFN[1] layer, which used a 30 min exposure (Fig. 1(b)). This suggests that a thicker and more hydrophobic layer results from greater exposure time of physFN on silicon oxide surfaces. The contact angle of the physFN[2] layer, of approximately 105°, is in reasonable agreement with literature values reporting it as $97.14° \pm 4.28°$ (Daoud et al., 2010). In addition, the thickness of the physFN layer increases with a higher concentration of fibronectin used, whereas the thickness of the chemFN layer is relatively consistent regardless of the fibronectin concentration (data not shown).

A well-known Rhodamine Red™-X, Succinimidyl Ester (Abs/Em = 560/581 nm), which reacts with residual amine functional groups of the lysine present in chemFN layers, was used in order to additionally confirm the immobilization of the fibronectin on the SiO$_2$ surfaces. Fig. S3 shows fluorescent images of rhodamine red treated GPTMS and chemFN QCM crystal surfaces. The control GPTMS surface is simply the underside of the chemFN-coated crystal. The Rhodamine Red treated fibronectin has a nearly 5-fold increase in fluorescence intensity as compared to that of GPTMS, 1355 ± 523 and 274 ± 146 ($p < 0.0001$), respectively (Fig. S3(b)). This indicates that fibronectin is chemically grafted to the GPTMS derivatized surface, and that the residual amine groups of the fibronectin grafted layer on the silicon oxide surface remain and react with the succinimidyl ester functional groups of Rhodamine Red™-X.

FTIR was also performed on GPTMS, physFN and chemFN surfaces (Fig. S4). Both chemFN and physFN display similar peaks at ~ 1639 cm^{-1} and 1536^{-1} which are not present in the GPTMS spectrum. These bands most likely correspond to the amide I and amide II groups observed in fibronectin by others at similar wavenumbers (Cheng et al., 1994), and provide further evidence that fibronectin is immobilized on the chemFN surface.

3.2. ChemFN and physFN surface characterization using AFM

To examine the surface differences between chemically chemFN and physFN layers on QCM sensors, the surface morphology and roughness of each dry surface was characterized using tapping mode AFM. Images were also taken of the GPTMS modified surface prior to chemFN coating (Fig. S5), with a resulting R_{rms} of 1.27 ± 0.31 nm. Fig. 2(a) and (b) show representative topography and phase-contrast images (1×1 μm^2 scan area) of chemFN and physFN layers on QCM sensors, respectively. Images of the chemFN layer show circular domains with a diameter of ~ 50 nm, and nanocrystalline particle shapes are observed in the phase image. The R_{rms} of the chemFN surface is 2.24 ± 0.68 nm (Fig. 2(c)). In contrast, the particle domains are not observed on the physFN surfaces, with an R_{rms} of 1.72 ± 0.22 nm ($p = 0.007$ vs. chemFN surfaces). This value is characteristic of a surface that is smooth and rather featureless, and is in reasonable agreement with literature values (Daoud et al., 2010). This suggests that fibronectin fills in the valleys between the particle domains, an assumption which is supported by the SE results reporting a greater thickness resulting from physFN deposition. Despite the difference in roughness between the two surfaces, the low R_{rms} values for both chemFN and physFN indicate that both of these surfaces are extremely smooth.

Overall, the surface characterizations of the chemFN and physFN layers show that the chemFN layer is thinner, rougher at the nanoscale, and more hydrophilic than the physFN layer. To evaluate our method of chemically coating fibronectin in cell culture applications, we studied how the chemFN surface affects cell culturing as compared to physFN layers.

3.3. Biocompatibility evaluation of chemFN surfaces

3.3.1. Cell metabolic activity and cytoskeletal structure
To confirm the viability of cells on both chemFN and physFN surfaces, cells were stained with calcein-AM. Cells from both surfaces displayed similar calcein staining, suggesting that HUVEC viability is similar on both surfaces (Fig. 3(a)). In addition, cells on both surfaces displayed normal cytoskeletal morphologies with visibly aligned phalloidin-stained actin filaments (Fig. 3(a)). While the chemFN surfaces shown in the figures were plated on glass coverslips, similar results were found with chemFN surfaces plated on silicon oxide or QCM crystals (data not shown).

3.3.2. Cell adhesion and adhesion strength
To compare the ability of cells to adhere to chemFN and physFN surfaces, cells were seeded at a density of 10,390 cells/cm^2. On chemFN surfaces cells adhered at a density of 10,270 cells/cm^2 after 3 h, while the physFN surface had 9790 cells/cm^2. Thus, the number of seeded cells was almost completely recovered on both surfaces. This experiment was repeated three more times with similar results, with cells on average adhering to chemFN $98.25 \pm 10.45\%$ ($p = 0.615$) as much as to physFN. Cell adhesion is thus not statistically different on the two surfaces.

HUVEC were also placed in flow chambers in order to test whether adhesion strength of cells plated on both surfaces was similar. Shear stress was increased stepwise to a maximum of
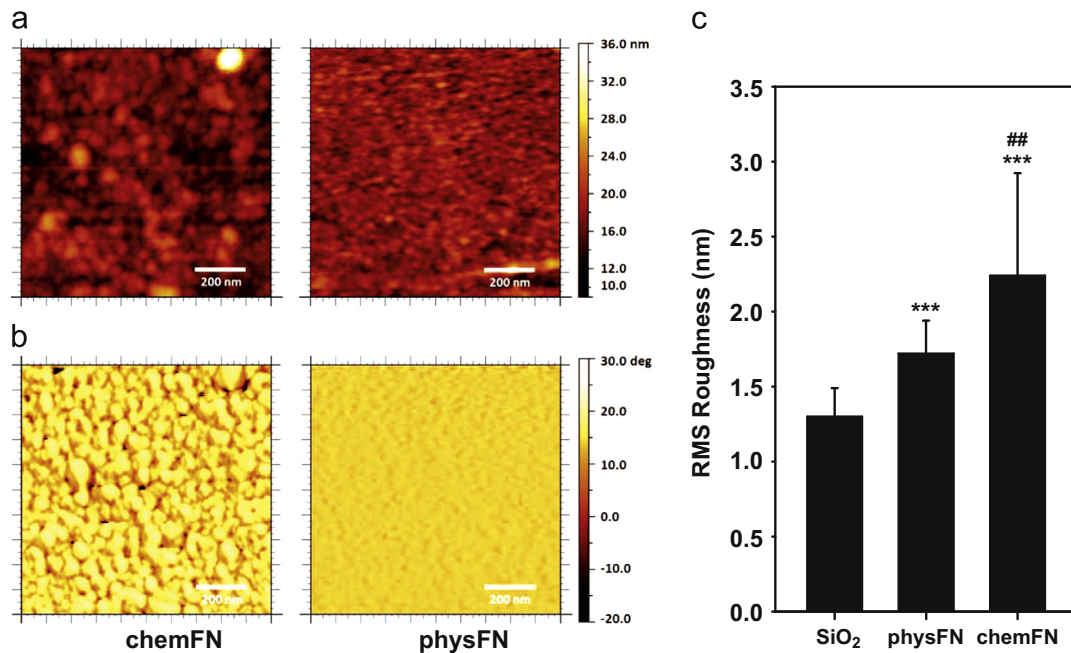
Fig. 2. (a) Topology and (b) phase AFM images of chemFN and physFN on SiO_2 coated QCM sensors, respectively. The scan area of each image shown is $1 \times 1 \, \mu m^2$. (c) RMS roughness of SiO_2, physFN, and chemFN surfaces. RMS roughness is reported as mean $\pm$ SD. Roughness values were determined from 25 separate $1 \, \mu m^2$ subsections taken from $5 \times 5 \, \mu m^2$ images for each substrate type. [##]represents $p < 0.001$ versus physFN, [***]represents $p < 0.0001$ versus the SiO_2 surface, with $p < 0.05$ considered to be significantly different.
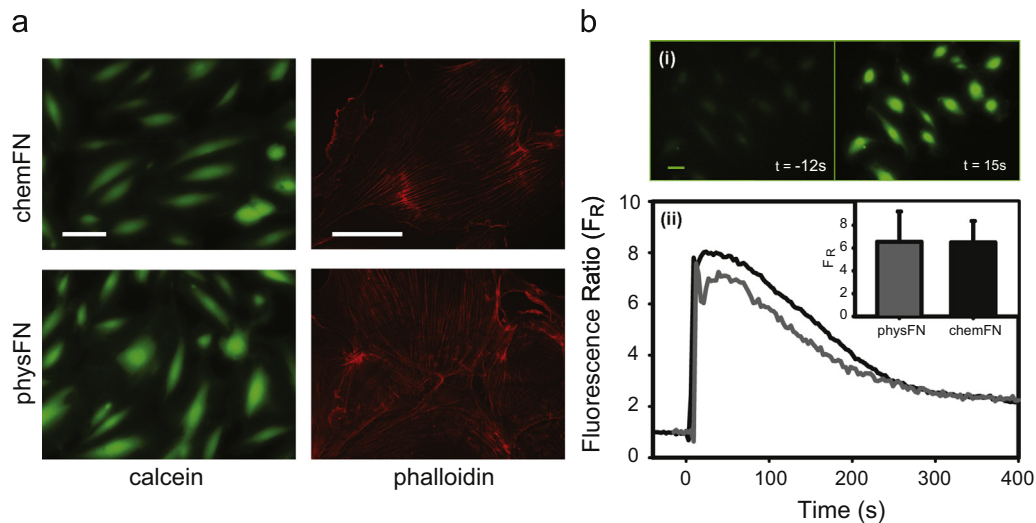
Fig. 3. (a) Calcein (vital dye) and phalloidin (actin dye) stained cells on chemFN and physFN surfaces. The brightness-contrast of the calcein images was adjusted to show the same range of intensities. All scale bars are 100 μm. Calcein images were taken with a $20 \times$ objective lens, and phalloidin images were taken with a $60 \times$ oil-immersion objective. (b) ATP stimulation of fluo-4 loaded cells. (i) A group of fluo-4 labeled chemFN cells before and after stimulation with ATP. $T = 0$ is considered to be when the ATP is added to the dish. Scale bar is 20 μm. (ii) Representative traces of the calcium signal of a cell plated on a chemFN surface (black) and a physFN surface (gray). Inset: average fluorescence ratios for all responding cells on chemFN (44/49) and physFN (34/36) surfaces. A Student's t-test comparing the two groups gave $p = 0.91$.

52 dyne/cm², and no cell detachment from either chemFN or physFN was observed. Some have reported that forces as high as ~500 dyne/cm² are required to detach cells (Gallant et al., 2005), so our experiments do not definitively establish that adhesion strength is identical on the two surfaces. At higher levels of shear stress, cell adhesion may be influenced by the differences in surface hydrophilicity between the two surfaces, though it is not clear exactly how (see Bacakova et al. (2011) for a review). For practical QCM-D experimentation, though, the fact that HUVECs did not detach from chemFN or physFN surfaces at shear levels corresponding to high physiological arterial shear stress levels (Malek et al., 1999) demonstrate that cell adhesion is sufficiently robust on both types of surfaces.

3.3.3. Cell proliferation

AlamarBlue was also used in order to assess cell viability, proliferation and metabolism. ChemFN cells gave alamarBlue fluorescence intensities of $88.4 \pm 13.3\%$ the intensity of control physFN cells plated at the same density. This number represents the mean of three separate experiments performed on different days. A resulting p-value of 0.200 indicates that metabolic activity of cells plated on both surfaces is similar.

3.3.4. Calcium release in response to addition of extracellular ATP

A final assessment of cellular health on chemFN and physFN surfaces measured the release of intracellular calcium in response

to the addition of extracellular ATP. In the physFN group, 34/36 (94.4%) cells responded to extracellular ATP addition with calcium transients, and in the chemFN group, 44/49 (89.8%) cells responded. Data are pooled from multiple experiments divided over two separate days. Fig. 3(b,i) shows a group of fluo-4 loaded chemFN cells before and after ATP stimulation, while Fig. 3(b,ii) shows representative traces of the calcium signal of a sample chemFN cell and a physFN cell. The inset of Fig. 3(b,ii) shows the mean F_Rs and standard deviations for all responding cells measured from both groups. The mean F_R for physFN cells was 6.55, while for chemFN cells it was 6.49, with a Student's t-test giving $p = 0.9097$. This indicates that the cellular responses on both surfaces were virtually identical.

3.4. QCM-D

There were three stages to data collection in the QCM-D experiments with cells (see Methods section, Fig. 5(a)). Stage I involved obtaining a baseline of the coated chemFN or physFN crystal, stage II measured the properties of the same crystal with adherent cells, and stage III involved measuring the crystal after removing the fibronectin and adherent cell layers. To estimate the physical properties of both the fibronectin layer and the adherent cell layer, frequency and dissipation data were stitched together in the order III–I–II, followed by modeling using the QTools software, as shown in Fig. 4. Both Fig. 4(a) and (b) show good fits for all three vibrational modes displayed for both physFN and chemFN surfaces. After modeling, Fig. 4(c) shows that the thickness of the physFN layer in PBS solution is 76 nm and that the layer thickness after subsequent cell culture increases to 94 nm. Fig. 4(d) shows that the viscosity and shear modulus of the crystal with cells are lower than those of physFN layer before cell adhesion: the viscosity decreases from 3.93 to 2.84×10^{-3} Ns/m^2, while the shear modulus decreases from 16.1×10^4 N/m^2 to 12.6×10^4 N/m^2. The increased thickness of physFN as compared to chemFN coupled with our observation that prolonged rinsing affects the physFN surface makes it impossible to determine whether the changes in thickness, viscosity and shear modulus are solely attributable to the
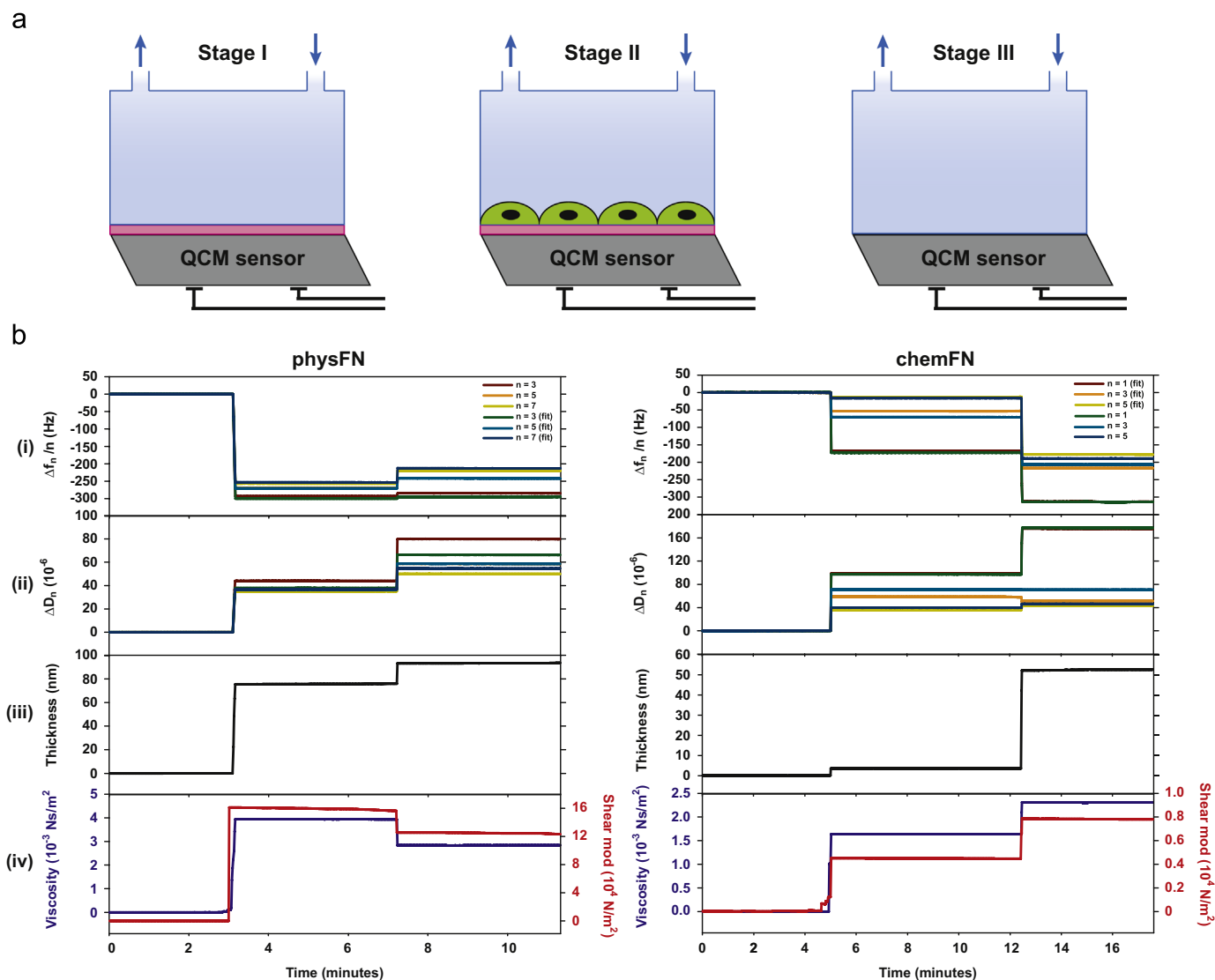
Fig. 4. (a) Experimental scheme for data collection using QCM-D. Stage I: Collecting frequency (Δf) & dissipation (ΔD) data using chemFN or physFN coated QCM sensors and PBS solution (flow rate = 100 μL/min, 21 °C); stage II: collecting Δf and ΔD using the QCM-sensor from stage I with cells under the same conditions as stage I; stage III: collecting Δf and ΔD using the cleaned SiO$_2$-coated QCM sensor with the same conditions as stage I. (b) Overall combined traces of (i) $\Delta f_n/n$ ($n = 3, 5, 7$) and (ii) ΔD_n of a cleaned SiO$_2$-coated QCM sensor (stage III), the fibronectin layer on a SiO$_2$-coated QCM sensor (stage I), and the cell adherent layer on representative physFN and chemFN QCM-D sensors (stage II) in PBS. The data from stages I, II, and III were stitched together for modeling in the order III–I–II using Q-soft (Q-Sense). Simulated and experimental curves for $\Delta f_n/n$ ($n = 3, 5, 7$) and ΔD_n vs. time show a good fit between the viscoelastic model and the experimental data. (iii) Thickness of the fibronectin and cell layers in PBS as determined from the fits shown in (i) and (ii). (iv) Viscosity and shear modulus of the fibronectin and cell layers as determined from the fits shown in (i) and (ii).
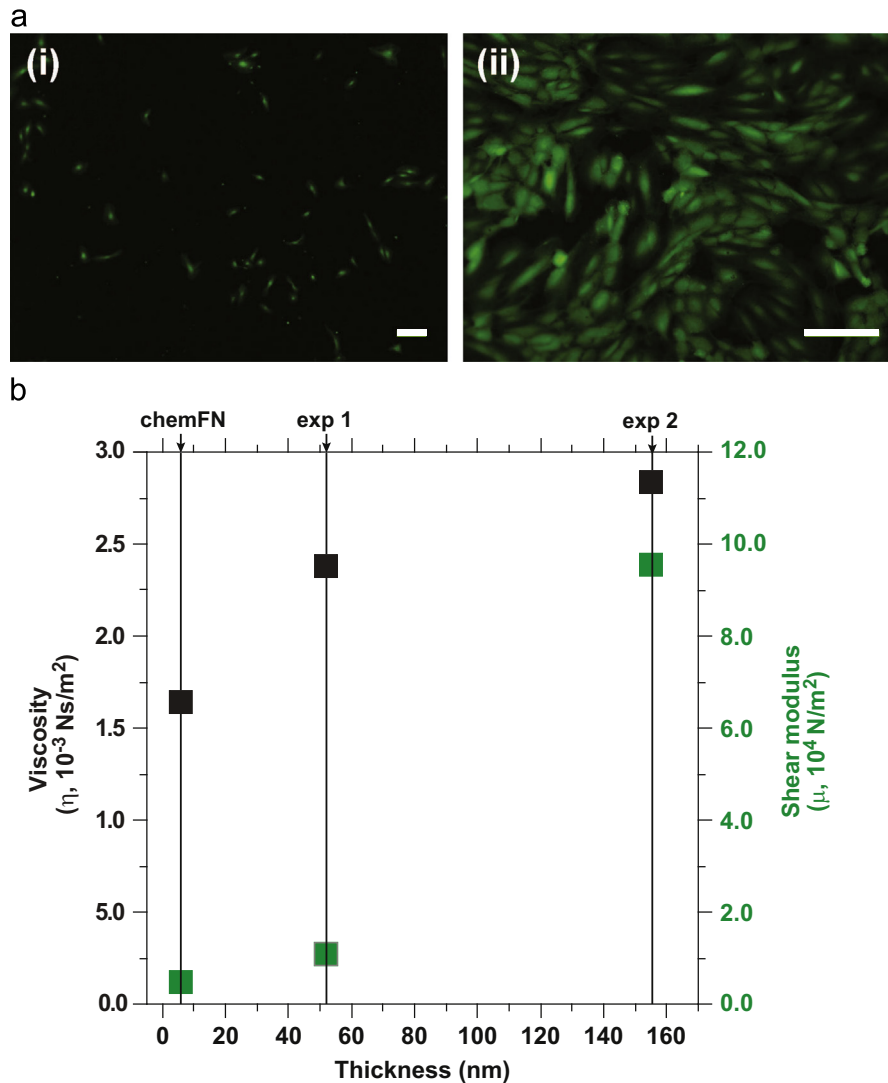
Fig. 5. (a) Representative fluorescent images of (i) low cell density (753 cells/cm^2) and (ii) high cell density (24,448 cells/cm^2) on chemFN QCM sensors, respectively. Both scale bars are 200 μm. The image shown in (i) was taken at $4\times$, while the image shown in (ii) was taken at $10\times$. (b) Viscosity (black) and shear modulus (gray) versus thickness of the cell layer on the chemFN layer. Exp 1 corresponds to (a(i)) and exp 2 corresponds to (a(ii)). The properties of the chemFN layer (derived from exp 1) are as follows: *in-situ* thickness=6 nm, viscosity=1.64×10^{-3} Ns/m^2, shear modulus=0.45×10^4 N/m^2.

cellular environment rather than changes in the fibronectin layer as well.

The right side of Fig. 4 displays an example of the QCM data modeling cell adhesion using a chemFN coated QCM sensor. Fig. 4 (c) shows that the thickness of the chemFN layer in PBS solution is 6 nm, increasing to 52 nm after cell culture. This indicates that chemFN swells in PBS, since SE measured the dry thickness of the chemFN layer at 3.0 ± 0.5 nm (Fig. 1(b)). The thickness increase after cell culture, 46 nm in this particular experiment, can be attributed to the cellular environment because of the stability of the chemically bonded fibronectin layer. In addition, since the chemFN layer is so thin to begin with, there is little worry that cell deposition is responsible for much more than the 46 nm thickness increase even if chemFN removal was to occur. Fig. 4(d) shows the viscosity and shear modulus of the chemFN layer before cell adhesion to be 1.64×10^{-3} Ns/m^2 and 0.453×10^4 N/m^2, respectively, which increase to 2.38×10^{-3} Ns/m^2 and 1.07×10^4 N/m^2, respectively, after cell culture. Fig. 5(a,i) shows a representative fluorescence image of calcein-stained adherent cells on the chemFN-coated sensor following the collection of the QCM data shown in Fig. 4, stage II. The staining demonstrates cell viability,

and gives the measured cell density for this particular experiment as 753 cells/cm^2 (Table S1).

To study how cell density affects the modeled thickness, viscosity and shear modulus, we performed another QCM-D experiment using a much higher cell concentration. The cleaning step (stage III) was not performed for this experiment, so only the properties of the cellular environment were measured. Fig. 5(a,i) and Table S1 give the measured cell density as 24,450 cells/cm^2 and the estimated thickness, viscosity, and shear modulus of the adherent cell layer as 155 nm, 2.84×10^{-3} Ns/m^2, 9.53×10^4 N m^2, respectively. The actual values of viscosity and shear modulus are not physiologically relevant, since the Voigt model used for QCM modeling is far too simplified for complex biological systems and better models do not currently exist (Tymchenko et al., 2012). However, when comparing samples to one another, viscosity and shear modulus indeed increase with increased cell density as expected (Fig. 5(b)), demonstrating that these values are meaningful in the relative sense. Again, because the chemFN layer is thin and stable, we can be confident that the signal change from stage I to stage II in these experiments is indeed solely attributable to the cell adherent layer and its surrounding environment rather than to changes in the fibronectin layer as well.
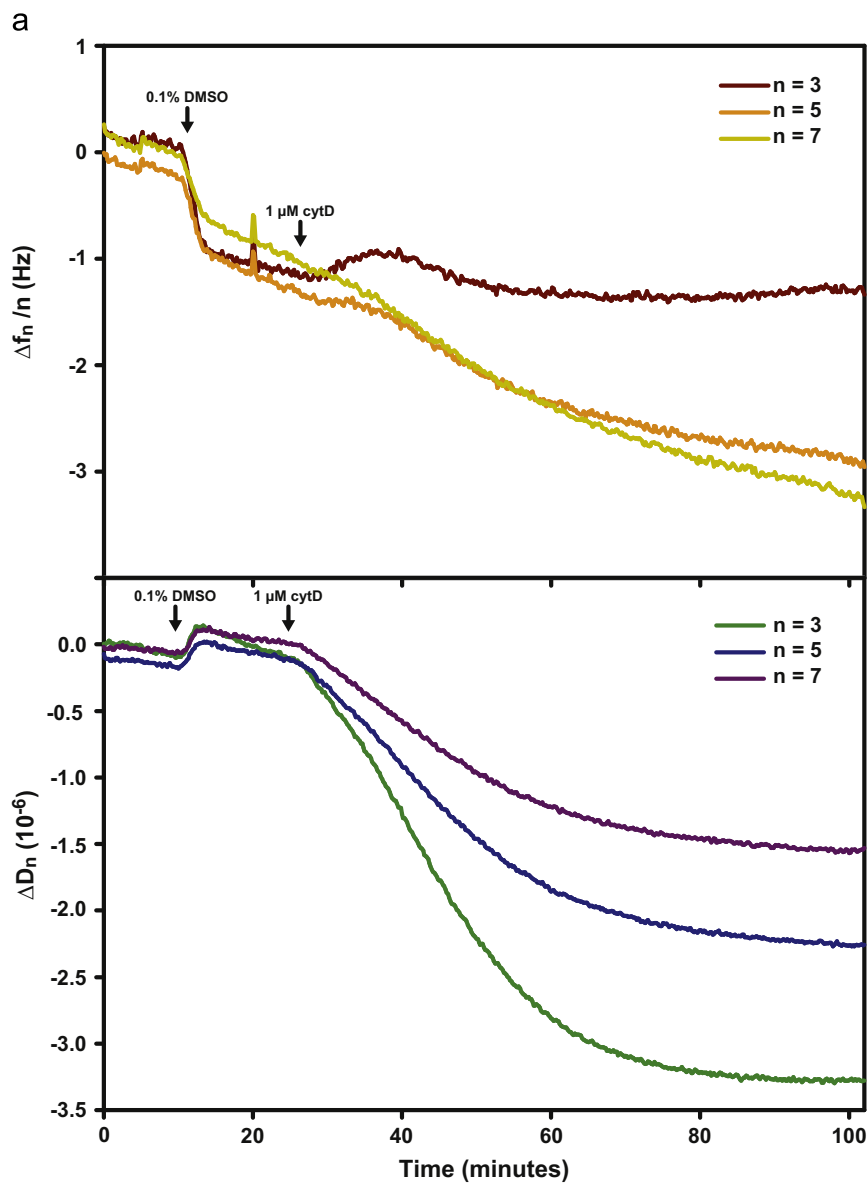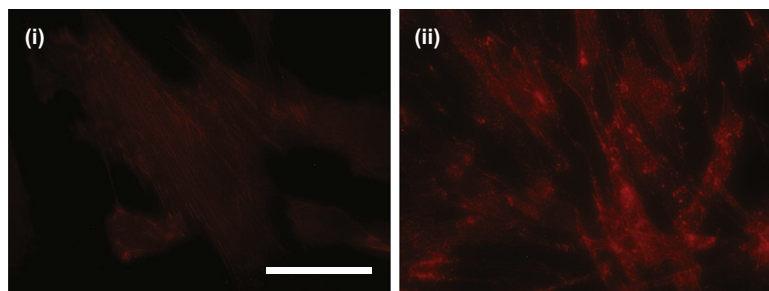
Fig. 6. (a) Real-time frequency and dissipation changes of a chemFN coated crystal plated with fibroblasts and then subjected to 1 μM cytD. (b) Fibroblasts stained with phalloidin to highlight the actin cytoskeleton. (i) Shows control cells on a crystal treated with 0.1% DMSO only, while (ii) shows cells on the crystal treated with cytD. The scale bar is 20 μm.

We also used the chemFN method in order to investigate real-time changes in QCM-D frequency and dissipation in response to drug-induced changes in cellular viscoelasticity. While frequency changes were negligible, a characteristic decrease in dissipation was observed in fibroblasts treated with 1 μM cytD (Fig. 6(a)) in agreement with others' observations (Saitakis et al., 2010, Wegener et al., 2000). Fig. 6(b,i) shows normal actin filament staining of cells on a crystal treated only with 0.1% DMSO, while Fig. 6(b,ii) shows the

disrupted actin filaments of the cells on the crystal subjected to cytD. No such dissipation decrease was observed for the crystal shown in Fig. 6(b,i) (data not shown), indicating that the mechanical changes were due to cytD alone. Likewise, no changes in dissipation or frequency were observed when cytD was added to a chemFN crystal without cells (data not shown). These data demonstrate that the chemFN method yields biofunctionalized QCM crystals which preserve the ability of QCM-D to sense real-time cellular mechanical

changes. The dissipation decrease observed implies cell stiffening. This does not inherently contradict AFM data showing cell softening in response to cytD treatment (Rotsch and Radmacher, 2000) since different portions of the cell are being interrogated by these two different methods. The results may imply that the basal region of the cell, which is accessed by QCM-D, reacts to actin depolymerization in a totally different manner than does the upper cellular region, which is accessed by AFM.

4. Conclusions

We have demonstrated a novel method of chemical immobilization of fibronectin onto various surfaces, including glass, quartz, and silicon. A cell culture model system has shown that cells are similarly healthy on these surfaces as those plated on the traditionally used, physisorbed fibronectin coating. Our surface characterization and QCM results indicate that the chemFN surfaces are thinner and more stable than the physFN ones, properties which are both critical in maximizing detection and repeatability in QCM research. Finally, we show that the presence of cells on the chemFN surface leads to an expected increase in measured thickness, viscosity and shear modulus of the crystal, and that this effect is intensified in the presence of an even greater cell density. These experiments involve the extraction of cellular mechanical properties from repeated measures of a single crystal, a capability which in the future will allow for the mechanical comparison of different groups of cells. We also presented characteristic real-time dissipation changes occurring with cells subjected to cytochalasin D on a chemFN coated crystal surface. These data suggest the potential for future real-time QCM-D experiments using chemFN for surface functionalization. All of these results demonstrate the excellent suitability of chemFN surfaces for QCM research, and we anticipate that the use of our method will greatly expand the capability of QCM experimentation within the increasingly broad field of cell mechanics. In addition, we hope that the experimental improvement constituted by the chemFN method will inspire the development of better QCM-D models appropriate for cellular experimentation.

Acknowledgments

Appendix A. Supplementary material

Supplementary data associated with this article can be found in the online version at http://dx.doi.org/10.1016/j.bios.2014.02.053.

References

Bacakova, L., Filova, E., Parizek, M., Ruml, T., Svorcik, V., 2011. Biotechnol. Adv. 29, 739–767.
Campoccia, D., Montanaro, L., Arciola, C.R., 2013. Biomaterials 34, 8533–8554.
Chen, J.Y., Shahid, A., Garcia, M.P., Penn, L.S., Xi, J., 2012. Biosens. Bioelectron. 38, 375–381.
Cheng, S.-S., Chittur, K.K., Sukenik, C.N., Culp, L.A., Lewandowska, K., 1994. J. Colloid Interface Sci. 162, 135–143.
Coll Ferrer, M.C., Eckmann, U.N., Composto, R.J., Eckmann, D.M., 2013. Toxicol. Appl. Pharmacol. 272, 703–712.
Cross, S.E., Jin, Y.-S., Rao, J., Gimzewski, J.K., 2007. Nat. Nanotechnol. 2, 780–783.
Daoud, J., Petropavlovskaia, M., Rosenberg, L., Tabrizian, M., 2010. Biomaterials 31, 1676–1682.
Darling, E.M., Topel, M., Zauscher, S., Vail, T.P., Guilak, F., 2008. J. Biomech. 41, 454–464.
Dastgheyb, S.S., Eckmann, D.M., Composto, R.J., Hickok, N.J., 2013. J. Photochem. Photobiol. B: Biol. 129, 27–35.
Eckmann, D.M., Tsai, I.Y., Tomczyk, N., Weisel, J.W., Composto, R.J., 2013. Colloids Surf. B: Biointerfaces 108, 44–51.
Elsom, J., Lethem, M.I., Rees, G.D., Hunter, A.C., 2008. Biosens. Bioelectron. 23, 1259–1265.
Fredriksson, C., Kihlman, S., Rodahl, M., Kasemo, B., 1998. Langmuir 14, 248–251.
Frisch, S.M., 1996. J. Cell Biol. 134, 793–799.
Gallant, N.D., Michael, K.E., García, A.J., 2005. Mol. Biol. Cell 16, 4329–4340.
Hermanson, G.T., 1996. Bioconjugate Techniques. Academic press, San Diego, CA.
Höök, F., Kasemo, B., Nylander, T., Fant, C., Sott, K., Elwing, H., 2001. Anal. Chem. 73, 5796–5804.
Ingber, D.E., Folkman, J., 1989. J. Cell Biol. 109, 317–330.
Jhon, Y.K., Bhat, R.R., Jeong, C., Rojas, O.J., Szleifer, I., Genzer, J., 2006. Macromol. Rapid Commun. 27, 697–701.
Jia, F., Narasimhan, B., Mallapragada, S., 2014. Biotechnol. Bioeng. 111, 209–222.
Kent, N.J., Basabe-Desmonts, L., Meade, G., MacCraith, B.D., Corcoran, B.G., Kenny, D., Ricco, A.J., 2010. Biomed. Microdevices 12, 987–1000.
Klinger, A.L., Pichette, B., Sobolewski, P., Eckmann, D.M., 2011. Integr. Biol. 3, 1033.
Lee, H.-S., Eckmann, D.M., Lee, D., Hickok, N.J., Composto, R.J., 2011. Langmuir 27, 12458–12465.
Lee, H.-S., Penn, L.S., 2008. Macromolecules 41, 8124–8129.
Lee, H.-S., Stachelek, S.J., Tomczyk, N., Finley, M.J., Composto, R.J., Eckmann, D.M., 2013a. J. Biomed. Mater. Res. Part A 101A, 203–212.
Lee, H.-S., Tomczyk, N., Kandel, J., Composto, R.J., Eckmann, D.M., 2013b. J. Mater. Chem. B 1, 6382–6391.
Lee, H.-S., Tsai, S., Kuo, C.-C., Bassani, A.W., Pepe-Mooney, B., Miksa, D., Masters, J., Sullivan, R., Composto, R.J., 2012a. J. Colloid Interface Sci. 385, 235–243.
Lee, H.-S., Yee, M.Q., Eckmann, Y.Y., Hickok, N.J., Eckmann, D.M., Composto, R.J., 2012b. J. Mater. Chem. 22, 19605–19616.
Lee, M.H., Ducheyne, P., Lynch, L., Boettiger, D., Composto, R.J., 2006. Biomaterials 27, 1907–1916.
Malek, A.M., Alper, S.L., Izumo, S., 1999. JAMA 282, 2035–2042.
Marx, K.A., Zhou, T., Montrone, A., McIntosh, D., Braunhut, S.J., 2007. Anal. Biochem. 361, 77–92.
Meyers, S.R., Grinstaff, M.W., 2012. Chem. Rev. 112, 1615–1632.
Miranti, C.K., Brugge, J.S., 2002. Nat. Cell Biol. 4, E83–E90.
Modin, C., Stranne, A.-L., Foss, M., Duch, M., Justesen, J., Chevallier, J., Andersen, L.K., Hemmersam, A.G., Pedersen, F.S., Besenbacher, F., 2006. Biomaterials 27, 1346–1354.
Ostuni, E., Kane, R., Chen, C.S., Ingber, D.E., Whitesides, G.M., 2000. Langmuir 16, 7811–7819.
Pankov, R., Yamada, K.M., 2002. J. Cell Sci. 115, 3861–3863.
Pelling, A.E., Veraitch, F.S., Chu, C.P.-K., Mason, C., Horton, M.A., 2009. Cell Motil. Cytoskelet. 66, 409–422.
Pierschbacher, M.D., Ruoslahti, E., et al., 1984. Nature 309 (30).
Pytela, R., Pierschbacher, M.D., Ruoslahti, E., 1985. Cell 40, 191–198.
Rotsch, C., Radmacher, M., 2000. Biophys. J. 78, 520–535.
Saitakis, M., Gizeli, E., 2011. Cell. Mol. Life Sci. 69, 357–371.
Saitakis, M., Tsortos, A., Gizeli, E., 2010. Biosens. Bioelectron. 25, 1688–1693.
Sauerbrey, G.Z., 1959. J. Physik 155, 206–212.
Shirtcliffe, N.J., Toon, R., Roach, P., 2013. Microfluidic Diagnostics. In: Jenkins, G., Mansfield, C.D. (Eds.), Humana Press, Totowa, NJ, pp. 241–268.
Sobolewski, P., Kandel, J., Klinger, A.L., Eckmann, D.M., 2011. Am. J. Physiol., Cell Physiol. 301, C679–686.
Takada, Y., Huang, C., Hemler, M.E., 1987. Nature 326, 607–609.
Tituhkin, I., Cho, M., 2007. Biophys. J. 93, 3693–3702.
Toworfe, G.K., Bhattacharyya, S., Composto, R.J., Adams, C.S., Shapiro, I.M., Ducheyne, P., 2009. J. Tissue Eng. Regen. Med. 3, 26–36.
Tymchenko, N., Nilebäck, E., Voinova, M.V., Gold, J., Kasemo, B., Svedhem, S., 2012. Biointerphases 7, 1–9.
Uttayarat, P., Perets, A., Li, M., Pimton, P., Stachelek, S.J., Alferiev, I., Composto, R.J., Levy, R.J., Lelkes, P.I., 2010. Acta Biomater. 6, 4229–4237.
Vig, J.R., Ballato, A., 1998. IEEE Trans. Ultrason. Ferroelectr. Freq. Control 45, 1123–1124.
Vogt, B.D., Lin, E.K., Wu, W., White, C.C., 2004. J. Phys. Chem. B 108, 12685–12690.
Völcker, N., Klee, D., Höcker, H., Langefeld, S., 2001. J. Mater. Sci.: Mater. Med. 12, 111–119.
Wegener, J., Seebach, J., Janshoff, A., Galla, H.-J., 2000. Biophys. J. 78, 2821–2833.
Xi, J., Chen, J.Y., Garcia, M.P., Penn, L.S., 2013. Biochip Tissue Chip, S5.
Zhou, T., Marx, K.A., Warren, M., Schulze, H., Braunhut, S.J., 2000. Biotechnol. Prog. 16, 268–277.